 CMC, vol.14, no.3, pp.209-219, 2009

Statistics of High Purity Nickel Microstructure From High Energy X-ray Diffraction Microscopy

C.M. Hefferan[1], S.F. Li[1], J. Lind[1], U. Lienert[2], A.D. Rollett[3] P. Wynblatt[3] and R.M. Suter[1,3]

Abstract: We have measured and reconstructed via forward modeling a small volume of microstructure of high purity, well annealed nickel using high energy x-ray diffraction microscopy (HEDM). Statistical distributions characterizing grain orientations, intra-granular misorientations, and nearest neighbor grain misorientations are extracted. Results are consistent with recent electron backscatter diffraction measurements. Peaks in the grain neighbor misorientation angle distribution at 60 degrees ($\Sigma 3$) and 39 degrees ($\Sigma 9$) have resolution limited widths of ≈ 0.14 degree FWHM. The analysis demonstrates that HEDM can recover grain and grain boundary statistics comparable to OIM volume measurements; more extensive data sets will lead to full, five parameter grain boundary character distributions. Due to its non-destructive nature, HEDM can then watch, both statistically and through tracking of individual grains and boundaries, the evolution of such distributions with processing of the sample.

Keywords: microstructure, high energy x-ray diffraction microscopy, synchrotron radiation, non-destructive orientation imaging

1 Introduction

Orientation imaging microscopy (OIM) is having a huge impact on microstructure science. Adams et al (1993); Rohrer (2005); Rohrer et al (2009) It allows measurements on the length scale of individual crystalline grains to replace bulk averages. Combined with serial sectioning, it yields three dimensional maps of grain orientations and geometries as well as corresponding grain boundary quantities. Lee (2007); Dillon and Rohrer (2009) OIM studies have lead to the development of a new metric for describing microstructures, the five parameter grain boundary

[1] Department of Physics, Carnegie Mellon University, Pittsburgh, PA USA.
[2] Advanced Photon Source, Argonne National Laboratory, Argonne, IL, USA.
[3] Materials Science and Engineering, Carnegie Mellon University, Pittsburgh, PA, USA.

character distribution (GBCD) and the ability to determine grain boundary energies and their distributions (GBED). Rollett et al (2001) It has been determined that the GBCD and GBED are correlated in many materials and that the GBED tends to be dominated by the grain boundary plane orientation rather than the grain-to-grain misorientation. Saylor (2004)

However, a clear shortcoming of OIM comes from the fact that it is a surface measurement. Gaining three dimensional information demands that the measured layers be stripped away to reveal the next layer. Several x-ray methods have been developed as alternatives to electron-based methods because x-rays can penetrate many materials and yield three dimensional information in a non-destructive way. Poulsen (2004); Poulsen et al (2001); Lienert et al (2009); Ludwig et al (2009); King et al (2008); Levine et al (2006); Larson et al (2005, 2002) High energy diffraction microscopy (HEDM) uses photons with energies greater than 40keV yielding penetration depths of tenths to tens of millimeters in a broad range of materials. Poulsen (2004); Poulsen et al (2001); Lienert et al (2007)

We report here on HEDM measurements of a well annealed nickel sample. We use our forward modeling approach to microstructure map generation. Suter et al (2008); Lienert et al (2007); Suter et al (2006) The point is to show that microstructure statistics comparable to those obtained with OIM are now accessible from a non-destructive measurement. Grain characteristics and grain neighbor misorientations are obtained that agree with recent OIM work. Li et al (2009) In this demonstration measurement, precise grain boundary plane orientations are not determined but this should be corrected in future data sets so that the full five parameter grain boundary character distribution will be available along with it's evolution with processing.

2 Procedure and Materials

Data were collected at beam line 1-ID of the Advanced Photon Source (APS). The facility and general procedures are described in the literature. Poulsen (2004); Poulsen et al (2001); Lienert et al (2007); Suter et al (2008, 2006) In this measurement we used 50 keV x-rays focused in the vertical to ≈ 2 μm height and the beam was 1.3 mm wide. A CCD based detector with 4×4 μm^2 sized pixels recorded diffraction images at rotation axis-to-detector distances of $L = 5.10, 7.10, 9.10$ mm. At each distance, 100 one degree oscillations were measured using three second exposure times.

The sample is a 1.1 mm diameter cylinder EDM cut from a larger block of high purity nickel. The cylinder length is ~ 4 cm and the measured volume is centered 1.04 mm from one of the ends. Prior to EDM, the block was annealed at 950 Centigrade

for six hours yielding grain sizes of roughly 40 microns as previously determined by serial sectioning and OIM Papillon and Wynblatt (2007). We measured nine planar cross-sections through the sample with ten micron separations. The measurement thus probes a volume of 0.063 mm^3 which should include $\sim$ 1000 grains.

Forward modeling reconstructions Suter et al (2008, 2006); Hefferan et al (2009) were carried out using Pittsburgh Supercomputing Center resources and a dedicated cluster at Carnegie Mellon. Each layer was treated independently and each element in the 2D triangular mesh for each layer was fitted independently. Adaptive regridding was used to reduce the computational burden. The smallest elements, which are used close to grain boundaries, had side lengths of 5.6 μm. A finer grid would only be meaningful with a higher resolution detector.Hefferan et al (2009)

Fig. 1 shows an example of one reconstructed layer which is analogous to an OIM surface measurement. The chief distinction is that this is a buried layer "sectioned" only by the non-destructive x-ray beam. This layer is meshed with 66,174 equilateral triangles of various sizes. The confidence, C, shown in Fig. 1b, is the fraction of simulated Bragg peaks generated by the fitted orientation that overlap experimental peaks in the HEDM data set. Typical orientations yield ≈ 40 Bragg peaks that strike at least two detectors, so even at $C = 0.35$, the reconstruction generates ~ 14 Bragg peaks that overlap experimentally observed intensity. C is reduced near grain boundaries due to noise in the shapes of experimental intensity profiles on the imaging detector.

With grain sizes of 40 microns and layer spacings of ten microns, one expects structural differences between adjacent layers to be significant but that most of the same grains will be sampled. This consistency is displayed in Fig. 2, where the maps of two adjacent layers have been overlapped and re-gridded, so that every triangle in one map has a one-to-one correspondence with a triangle in the adjacent map. The rotation angle required to bring the independently determined orientations in these overlapping mesh elements into coincidence is calculated and referred to as a misorientation. Locations in Fig. 2 of appreciable misorientation are principally at grain boundaries as expected. Careful inspection reveals a few grains that are observed in one layer but are out of the beam or much reduced in size in the adjacent layer.

The nine layers of reconstructed microstructure are combined into a single volumetric map which is used for the extraction of three-dimensional grain statistics. The triangular meshes referred to above are now interpreted as representing three dimensional "voxels" whose height extends from the measured layer halfway to the adjacent layers. Calculations are facilitated by a software analysis library (XDM++) that performs basic functions such as determining sets of voxels corresponding to a grain, boundaries between grains, connectivity information, and

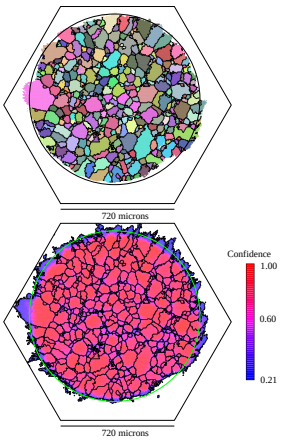

Figure 1: Microstructure map for one of the nine layers that compose the measured volume. (a) the orientation field and (b) the mesh element confidence, C. Orientations have been mapped to a color spectrum so that regions of similar color have similar crystallographic orientations. Black lines in the maps show mesh edges separating triangles with more than a two degree misorientation. The circles are guides to the eye showing the 1.1 mm diameter of the sample. (a) has been thresholded to include only mesh elements with $C > 0.35$. The hexagons are the reconstruction box.

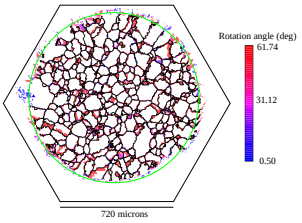

Figure 2: Element-to-element misorientation map comparing the layer shown in Fig. 1 and an adjacent one displaced by ten microns. Boundary lines (black) and the green circle are those of Fig. 1. Only misorientations greater than 0.5 degrees are drawn, hence regions that are inside the same grain in both layers are white. The layers contain mostly the same grains and the reconstruction of their orientations is consistent. Colors indicate the changes in cross-sectional shapes of the grains; blue regions cross low angle boundaries, red regions high angles.

a variety of statistical measures. Information about the relative locations of grains and boundaries is based on a connectivity graph in which grains and boundaries are represented by vertices and edges, respectively. Each vertex is assigned a single grain-averaged orientation which is computed from all member voxels. Cho et al (2004) Each edge is assigned the misorientation between the nodes it connects. Details of the XDM++ library will be published separately. Examples of statistics gathered from these routines are presented in the next section.

3 Results

Identifying contiguous sets of voxels with less than two degree misorientation, we identify 1101 grains in the measured volume that are comprised of more than 25 voxels or 136 μm^3 (which corresponds to a cube with 5.1 μm sides). The number of grains varies by less that one percent as the misorientation cut-off is varied by ± 1 degree. Fig. 3 shows the distribution of poles in stereographic projections and indicates only weak anisotropy. Fig. 4 shows that the annealed nickel grains are well ordered in that they typically have narrow internal misorientation distributions. The resolution of the measurement is roughly 0.1 degree. Hefferan et al (2009) Most grains have spreads only slightly larger than this while a few have more than 0.4 degree distribution widths.

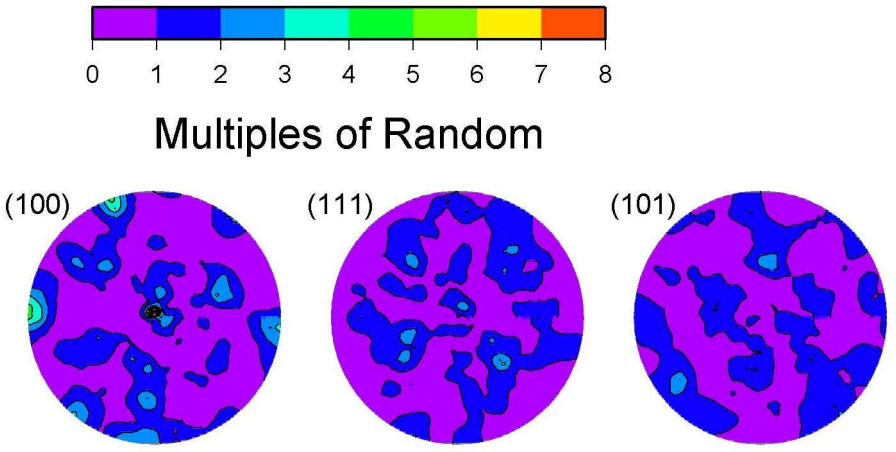

Figure 3: Pole figures for 1101 grains of the nickel microstructure. The distribution is largely random except for a weak peak of [100] axes along the cylinder axis of the rod-shaped sample.

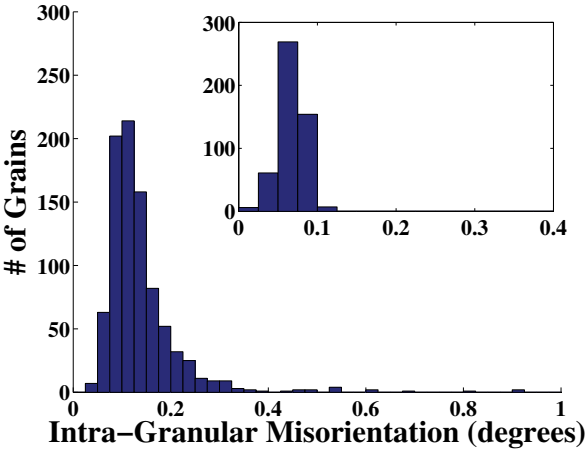

Figure 4: Intra-granular misorientation distribution. Insert: Similar statistic from a reconstruction of a simulated sample with 497 perfect grains (no internal misorientation) of similar size. In the simulation, no grains show more than 0.15 degree misorientation. Hefferan et al (2009)

Fig. 5 shows the distribution of misorientation angles between neighboring grains. Fig. 5(a) uses 0.1 degree bins since this is of the order of our orientation resolution. The broad (but noisy) distribution approximates the Mackenzie distribution of randomly oriented cubes. Mackenzie andThomson (1957) Two sharp peaks, at 39 ($\Sigma 9$) and 60 ($\Sigma 3$) degrees, are consistent with results from recent OIM measurements on a much smaller grained nickel polycrystal.Li et al (2009) As shown in the figure, these peaks have widths that are comparable to our measurement angular resolution. The distribution of rotation axes associated with misorientations of 60 ± 0.15 degrees is strongly peaked in the $[111]$ directions indicating that these are primarily twin boundaries that should have plane normals along $[111]$. Li et al (2009) This geometry leads to the asymmetric peak seen in Fig. 5b: due to the crystal symmetry, rotations by more than 60 degrees about $[111]$ are folded back below 60 degrees. A weaker peak (by a factor of ~ 8) in the 60 degree distribution occurs at $[110]$. Fig. 6 of reference Li et al (2009) shows that these are symmetric tilt boundaries with low interfacial energy.

Fig. 6 shows the set of axes corresponding to the $\Sigma 9$ misorientation angle of 39 degrees. The strong peaks at $[110]$ are associated with low energy asymmetric tilt boundaries.Li et al (2009) The appearance of peaks at several other axes requires further investigation using data sets that allow the determination of grain boundary

plane normals.

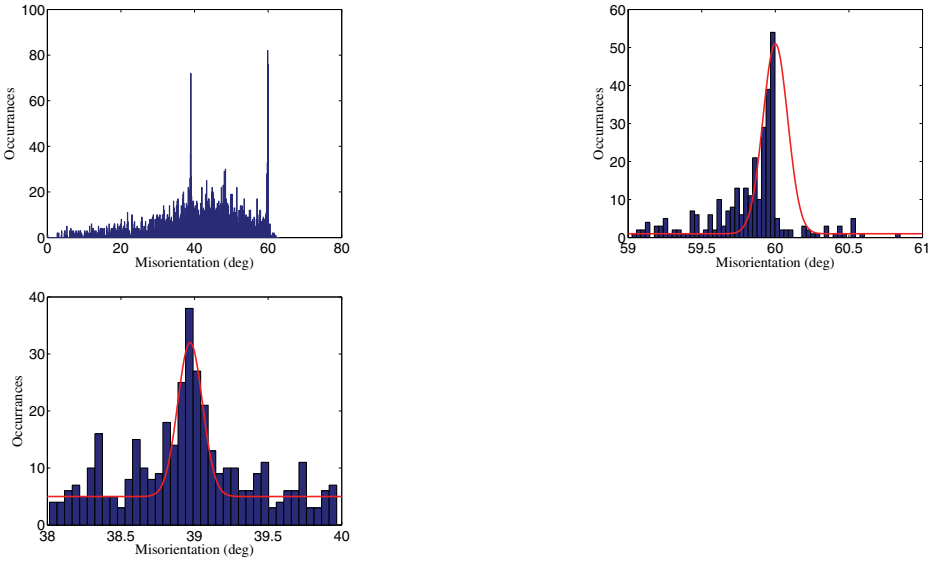

Figure 5: Histogram of nearest neighbor grain misorientation angles in the nickel data set. (a) shows the full angle range for cubic crystal symmetry using 0.1 degree bins. (b) shows the peak at 60 degrees and (c) the peak at 39 degrees on expanded scales. Curves in (b) and (c) are Gaussian guides to the eye with identical widths of 0.14 degree FWHM and center positions of 60.0 and 39.0 degrees, respectively.

4 Discussion

This note illustrates the point that HEDM microstructure mapping measurements are already at the point of yielding significant statistical information from ensembles of polycrystal grains. The number of grains measured here, ~ 1000, is comparable to three dimensional OIM data sets used for statistical analysis. Li et al (2009) The results summarized are entirely consistent with that analysis. It appears that the crystal orientation measurements using HEDM are more precise than those using backscattered electrons. This ~ 0.1 degree resolution is not machine limited – oscillation integration intervals smaller than one degree should yield an improvement. It appears from the narrow misorientation peaks of Fig. 5 that such resolution may be useful for some studies.

The intra-granular misorientation sensitivity demonstrated in Fig. 4 implies that defect content of individual grains can be resolved. It may be surprising that 0.1

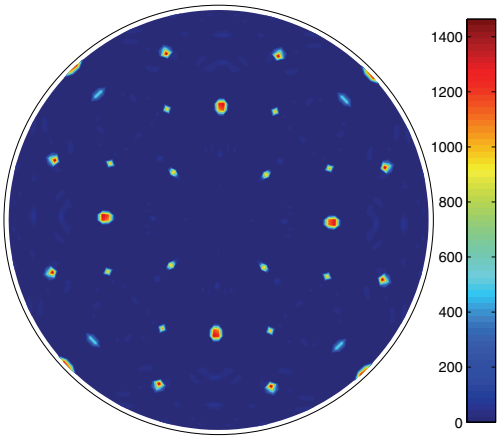

Figure 6: Stereographic projection of rotation axes associated with misorientations in the range 39 ± 0.15 degrees. The $[001]$ direction is at the center. Four fold symmetry has been enforced. A bin size of four degrees has been used for visual clarity; the actual peaks are no more than one degree wide.

degree orientation resolution can be obtained even using one degree integration intervals in data collection. However, the pixel resolution on the detector is at a distance from the origin of 500 pixels is of order 0.1 degree in both radial and azimuthal drections and, with many peaks being measured, this resolution is relevant for multiple sets of crystallographic planes. The finite size of diffraction spots from extended grains also limits angular resolution for voxels well inside the grains – the orientation can vary somewhat without moving simulated diffraction off the spots. However, for those peaks that generate scattering close to the horizontal plane (large $|\eta|$ in the notation of Refs. Suter et al (2008, 2006)) the projection geometry compresses the vertical size of diffraction spots confining the possible orientation variations. A defected grain with mosaic structure will spread these spots into finite height arcs (which further spread with increased detector distance, L) and onto detector images collected in adjacent integration intervals. These considerations are important for the interpretation of microstructure responses from grain growth to the imposition of strain.

What is lacking in this comparison to OIM are determinations of grain boundary plane orientations. We have not attempted this because in the current data, the inter-plane step size of ten microns is comparable to the grain size (40 μm). We have recently collected a large data set (from the same sample presented here) using

four micron increments and are developing analysis approaches for plane normal determination. Again, validation through comparison to reference Li et al (2009) will be performed.

The aim of developing HEDM is not to compete with or replace OIM. Synchrotron beam time available at the handful of appropriate beam lines in the world is much too limited. Rather, the point is to open the possibility to study the response of a few key microstructures on a grain-by-grain basis as materials are heat, strained, and/or treated chemically. The ability to obtain such detailed data on specific systems will help to constrain analytic and computational models and should lead to understanding that can be applied more generally. The present work, combined with that of other groups using non-destructive x-ray techniques, Lienert et al (2009); Ludwig et al (2009); King et al (2008); Levine et al (2006); Larson et al (2005, 2002) indicates that this scenario is reaching fruition.

Acknowledgement: This work was supported by the MRSEC program of the National Science Foundation under award number DMR-0520425 and NSF Metals program under award number DMR-0805100. Use of the Advanced Photon Source was supported by the U.S. Department of Energy, Office of Science, Office of Basic Energy Sciences, under Contract No. DE-AC02-06CH11357. This research was also supported in part by the National Science Foundation through TeraGrid resources provided by the Pittsburgh Supercomputing Center.

References

Adams, B.; Kunze, K.; Wright, S.I. (1993): Orientation Imaging: the emergence of a new microscopy. *Metallurgical and Materials Transactions,* vol. 24A, pp.819 – 831.

Cho, J.-H.; Rollett, A.D.; Oh, K.H. (2004): Determination of Volume Fractions of Texture Components with Standard Distributions in Euler Space. *Metallurgical and Materials Transactions,* vol. 35A, pp. 1075 – 1086.

Dillon, S.J.; Rohrer, G.S. (2009): Three-Dimensional FIB-OIM of Ceramic Materials. in *Applications of Texture Analysis,* A.D. Rollett, Editor, (Ceram. Trans., vol. 201, pp. 117-124, J. Wiley & Sons, Hoboken, NJ.

Hefferan, C.M.; Li, S.F.; Lind, J.; Suter,R.M. (2009): Tests of Microstructure Reconstruction by Forward Modeling of HEDM Data. *Advances in X-ray Analysis*, vol. 53, Proceedings of the Denver X-ray Conference, to be published.

King, A.; Johnson, G.; Engelberg, D.; Ludwig, W.; Marrow, J. (2008): Observations of Intergranular Stress Corrosion Cracking in a Grain-Mapped Polycrystal. *Science,* vol. 321, pp. 382-385.

Larson, B.C.; Yang, W.; Budai, J.D.; Tischler J.Z.; Pang, J.W.L.; Barabash, R.I.; Liu, W.; Ice, G.E. (2005): Polychromatic X-ray microdiffraction studies of mesoscale structure and dynamics. *J. Synchr. Rad.,* vol. 12, pp. 155-162.

Larson, B.C.; Yang, W.; Ice, G.E.; Budai J.D.; Tischler, J.Z. (2002): Three-dimensional X-ray structural microscopy with submicrometre resolution. *Nature,* vol. 415, pp. 887 – 890.

Lee, S.-B.; Rollett, A.D.; Rohrer, G.S. (2007): Three-dimensional Microstructure Reconstruction Using FIB-OIM. *Mat. Sci. Forum,* vols. 558-559, pp. 915 – 920.

Levine, L.E.; Larson, B.C.; Yang, W. (2006): X-ray microbeam measurements of individual dislocation cell elastic strains in deformed single-crystal copper. *Nature Mat.,* vol. 5, pp. 619-622.

Li, J.; Dillon, S.J.; Rohrer, G.S. (2009): Relative grain boundary area and energy distributions in nickel. *Acta Mat.,* vol. 57, pp. 4304 – 4311.

Lienert, U.; Almer, J.; Jakobsen, B.; Pantleon, W.; Poulsen, H.F.; Hennessy, D.; Xiao, C.; and Suter, R.M. (2007): 3-Dimensional Characterization of Polycrystalline Bulk Materials Using High-Energy Synchrotron Radiation. *Mat. Sci. Forum,* vols. 539-543, pp. 2353 – 2358.

Lienert, U.; Brandes, M.C.; Bernier, J.V.; Weiss, J.; Shastri, S.D.; Mills, M.J.; Miller, M.P. (2009): In-situ single grain peak profile measurements on Ti-7Al during tensile deformation. *Mat. Sci. and Engr. A,* vol. 524, pp. 46-54.

Ludwig, W.; Reischig, P.; King, A.; Herbig, M.; Lauridsen, E.M.; Johnson, G.; Marrow, T.J.; Buffiére, J.Y. (2009): Three-dimensional grain mapping by x-ray diffraction contrast tomography and the use of Friedel pairs in diffraction data analysis. *Rev. Sci. Instrum.,* vol. 80, pp. 033905.

Mackenzie, J.K.; Thomson, M.J. (1957): Some Statistics Associated with the Random Distribution of Cubes. *Biometrika,* vol. 44, pp. 205 – 210.

Papillon, F.; Wynblatt, P. (2007): unpublished.

Poulsen, H.F. (2004): *Three-Dimensional X-ray Diffraction Microscopy.* Springer.

Poulsen, H.F.; Nielsen, S.F.; Laurdisen, E.M.; Schmidt, S.; Suter, R.M.; Lienert, U.; Margulies, L.; Lorentzen, T.; Juul Jensen, D. (2001): Three-dimensional maps of grain boundaries and the stess state of individual grains in polycrystals and powders, *J. Appl. Cryst.,* vol. 34, pp. 751-756.

Rohrer, G.S. (2005): Influence of Interface Anisotropy on Grain Growth and Coarsening. *Annual Review of Materials Research,* vol. 35, pp. 99-126.

Rohrer, G.S.; Gruber, J.; Rollett, A.D. (2009): Distributions in polycrystalline materials. In *Materials Processing and Texture,* A. D. Rollett, ed. (Ceram. Trans., vol. 201, J. Wiley & Sons, Hoboken, NJ, 2009) pp. 343-354.

Rollett, A.D.; Yang, C.-C.; Mullins, W.W.; Adams, B.L.; Wu, C.T.; Kinderlehrer, D.; Ta'asan, S.; Manolache, F.; Liu, C.; Livshits, I.; Mason, D.; Talukder, A.; Ozdemir, S.; Casasent, D.; Morawiec, A.; Saylor, D.; Rohrer, G.S.; Demirel, M.; El-Dasher, B.; Yang W. (2001): Grain Boundary Property Determination through Measurement of Triple Junction Geometry and Crystallography. *Proceedings of the First Joint International Conference on Grain Growth,* Aachen, Germany, Eds. G. Gottstein and D.A. Molodov, (Springer Verlag, 2001) pp 165-175.

Saylor, D.M.; El-Dasher, B.S.; Pang, Y.; Miller, H.M.; Wynblatt, P.; Rollett, A.D.; Rohrer, G.S. (2004): Habits of Grains in Dense Polycrystalline Solids. *J. Amer. Ceram. Soc.,* vol. 87, pp. 724-726.

Suter, R.M.; Hefferan, C.M.; Li, S.F.; Hennessy, D.; Xiao, C.; Lienert, U.; Tieman, B. (2008): Probing Microstructure Dynamics With X-ray Diffraction Microscopy, *J. Eng. Mater. Technol.,* vol. 130, pp. 021007 1-5.

Suter, R.M.; Hennessy, D.; Xiao, C.; and Lienert, U. (2006): Forward Modeling Method for Microstructure Reconstruction Using X-ray Diffraction Microscopy: Single Crystal Verification. *Rev. Sci. Instr.,* vol. 77, 123905, pp. 1 – 12.